COVER SHEET

This is the author version of article published as:

Roberts, Peter J. and Walker, Rodney A. and O'Shea, Peter J. (2005) Tightly Coupled GNSS and Vision Navigation for Unmanned Air Vehicle Applications. In Proceedings Australian International Aerospace Congress, Melbourne, Australia.

Tightly Coupled GNSS and Vision Navigation for Unmanned Air Vehicle Applications

Mr Peter J Roberts[1], Dr Rodney A Walker[1] and Dr Peter O'Shea[2]

[1] *Airborne Avionics Research Group, Cooperative Research Centre of Satellite Systems, Queensland University of Technology, GPO Box 2434, Brisbane, 4001, Australia*
[2] *School of Electrical and Electronic Systems Engineering, Queensland University of Technology, GPO Box 2434, Brisbane, 4001, Australia*

Summary: This paper explores the unique benefits that can be obtained from a tight integration of a GNSS sensor and a forward-looking vision sensor. The motivation of this research is the belief that both GNSS and vision will be integral features of future UAV avionics architectures, GNSS for basic aircraft navigation and vision for obstacle-aircraft collision avoidance.

The paper will show that utilising basic single-antenna GNSS measurements and observables, along with aircraft information derived from optical flow techniques creates unique synergies.

Results of the accuracy of attitude estimates will be presented, based a comprehensive Matlab® Simulink® model which re-creates an optical flow stream based on the flight of an aircraft. This paper establishes the viability of this novel integrated GNSS/Vision approach for use as the complete UAV sensor package, or as a backup sensor for an inertial navigation system.

Keywords: UAV Navigation, Navigation Sensor, GNSS, Vision, Optic Flow, Sensor Fusion.

Introduction

This paper presents preliminary results of the research into a novel navigation sensor suite concept for use in UAV applications. This research is targeted towards satisfying the navigation needs of a fixed wing UAV platform through the use of GNSS and vision.

The broad objective of this research is to investigate the unique synergies that exist between GNSS and vision for fixed wing UAV navigation and control. Encompassed in this broad objective are two central areas of focus for the research and they are as follows:

1. Investigate the fusion of GNSS and vision techniques
    a. Develop a novel sensor suite concept focusing on reducing size, mass, cost and power over traditional sensor suites with the same capability
    b. Utilise GNSS to aid in vision based attitude determination
    c. Evaluate the performance of the novel sensor suite concept
2. Increase the robustness of the vision system
    a. Employ biologically inspired techniques
    b. Remove the need for horizon tracking for attitude determination

The outcome of this research will be an optimised sensor for a fixed wing UAV capable of being utilised for:

- Standalone navigation
- Sensor redundancy
- Sensor health monitoring

The motivation for the use of GNSS is the fact that advances in the field are expected to be achieved in the coming years, making GNSS an essential sensor for the majority of UAV applications. The motivation for the use of vision revolves around the need for UAV platforms to provide forced landing identification and collision detection capability. A human pilot uses vision as a key sensor for performing these tasks, and therefore it is logical that the UAV adopt a similar approach. The choice of these two sensors allows implementation of the concepts presented in this paper with minimal additional hardware.

This paper illustrates that in principal, this simple combination of GNSS and vision is sufficient to provide the desired information about the current state of the UAV and its surroundings.

Sensor Architecture

The typical approach to providing the navigation sensory needs for UAVs is to employ multiple dedicated sensors. Whilst being effective in providing the majority of the required navigation information it is inefficient in satisfying the size, mass, cost and power constraints that are usually imposed on UAV platforms.

The information that has been identified as desirable for the navigation of a UAV is contained in the following:

- Absolute position, velocity, time
- Roll, pitch and yaw angle
- Drift angle
- Height above ground
- Distance to objects in the field of view

There is a desire, and in some cases a need, to make sensors more intelligent and robust. This enables them to accommodate additional tasks that may not normally be associated with traditional navigation sensors.

This paper presents a novel sensor suite concept, utilising the synergies that exist between GNSS and vision, to provide a comprehensive navigation sensor suite.

GNSS Sensor Utilisation

It is imperative to the safe navigation of a UAV that the absolute position, velocity and time are known at any given instant. This knowledge is readily obtainable from a single antenna GNSS sensor. A GNSS sensor is well within the size, mass, power and cost limitations that are usually imposed on UAV platforms.

In addition to the absolute positioning gained from the GNSS sensor, accurate Doppler based velocity and derived acceleration measurements are utilised to provide an estimate of the

Euler angles and rates. It should be noted however that the Euler angles and rates derived from the GPS velocity relate directly to the attitude of the velocity vector and not to that of the UAV. Although this attitude information is not the final result, it is an integral part of the process to achieve it.

Vision Sensor Utilisation

Vision based sensors are a logical sensory component to a UAV as they can enable the UAV to mimic many of the processes performed by a human pilot. There have been several different approaches to utilising vision for UAV navigation sensors but they can generally be split into three main classes - horizon tracking, biologically based and biologically inspired.

The University of Florida have developed a horizon tracking method that uses a statistical approach to determining the separation between the sky and ground [1]. This method has successfully been implemented by R. Causey as part of an autopilot for a micro UAV [2]. This system has the limitation that the horizon must be in view.

Biologically based methods have been developed that use hardware based on that found in nature. A well researched example is the use of Elementary Motion Detectors (EMD) which are found on most flying insects. G. Barrows has successfully demonstrated the use of this technology in close proximity object detection for collision avoidance and altitude control [3-5]. These systems have the limitation that they require specialist hardware and have a restricted range.

Biologically inspired techniques exist that draw on the functionality of naturally occurring systems. Optic flow is one such method that has been derived from what is found in nature and provides very useful information, as shown in the research carried out by Javaan Chahl with rotary wing UAV platforms [3]. Optic flow calculations can be carried out on a standard image stream so that no specialised hardware is necessary.

The optic flow derived from the vision stream in the proposed sensor suite is utilised to determine the direction of the velocity vector in relation to the body frame of the UAV. The optic flow information is also used to estimate the distance to objects in the field of view.

GNSS and Vision Sensor Coupling

The GNSS and vision sensor combination lends itself to the derivation of many parameters useful for UAV navigation. The proposed sensor suite would have a size, mass, power and cost specification that is lower than that of a suite of traditional sensors that provide the same level of information. GPS is used to derive the attitude of the velocity vector of the UAV, vision to translate this derived attitude into the UAV body frame. This forms the basis of this novel sensor suite. The data flow throughout the novel sensor suite is illustrated in Fig. 1.

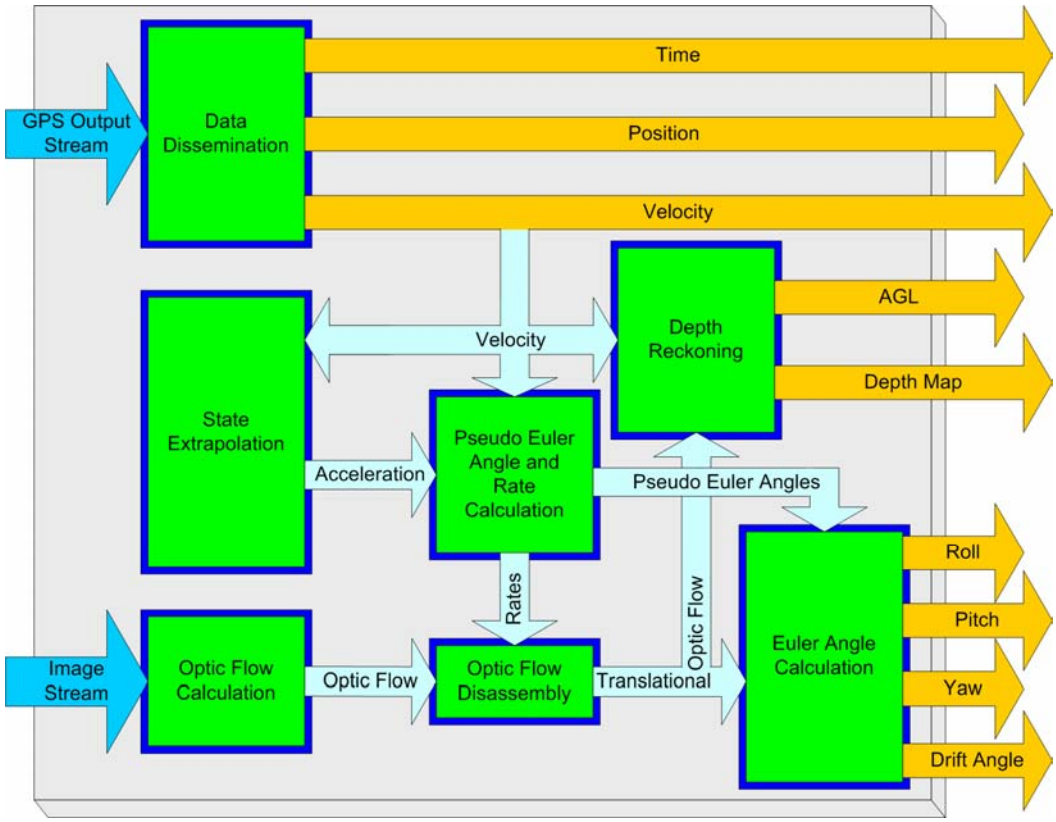

Fig. 1: Sensor Suite Overview

Each processing stage represented in Fig. 1 is explained and discussed in detail in the following sections.

State Extrapolation

During the processing of the pseudo roll angle and rate the GPS derived acceleration is required, this being the prime function of this processing stage. The derivative with respect to (wrt) time of the accurate Doppler based velocity measurements is taken to provide the acceleration vector.

Optic Flow Calculation

The optic flow between successive frames of the image stream is calculated in this processing stage. This will be a very processor intensive stage. Emphasis will therefore be placed on achieving an efficient and robust optic flow algorithm. The most likely candidate is a modification of the Lucas and Kanade algorithm [6] to take into account the relatively large motion that could occur between frames. Optic flow is essentially a measurement of the change in position of a point from one image frame to another. Fig. 2 shows the optic flow that is created from two image frames from an aircraft with a downward looking camera. The general trend of the optic flow closely matches the motion between images. The edge of the optic flow map contains erroneous results inherent in the optic flow algorithm and should be disregarded in can processing.

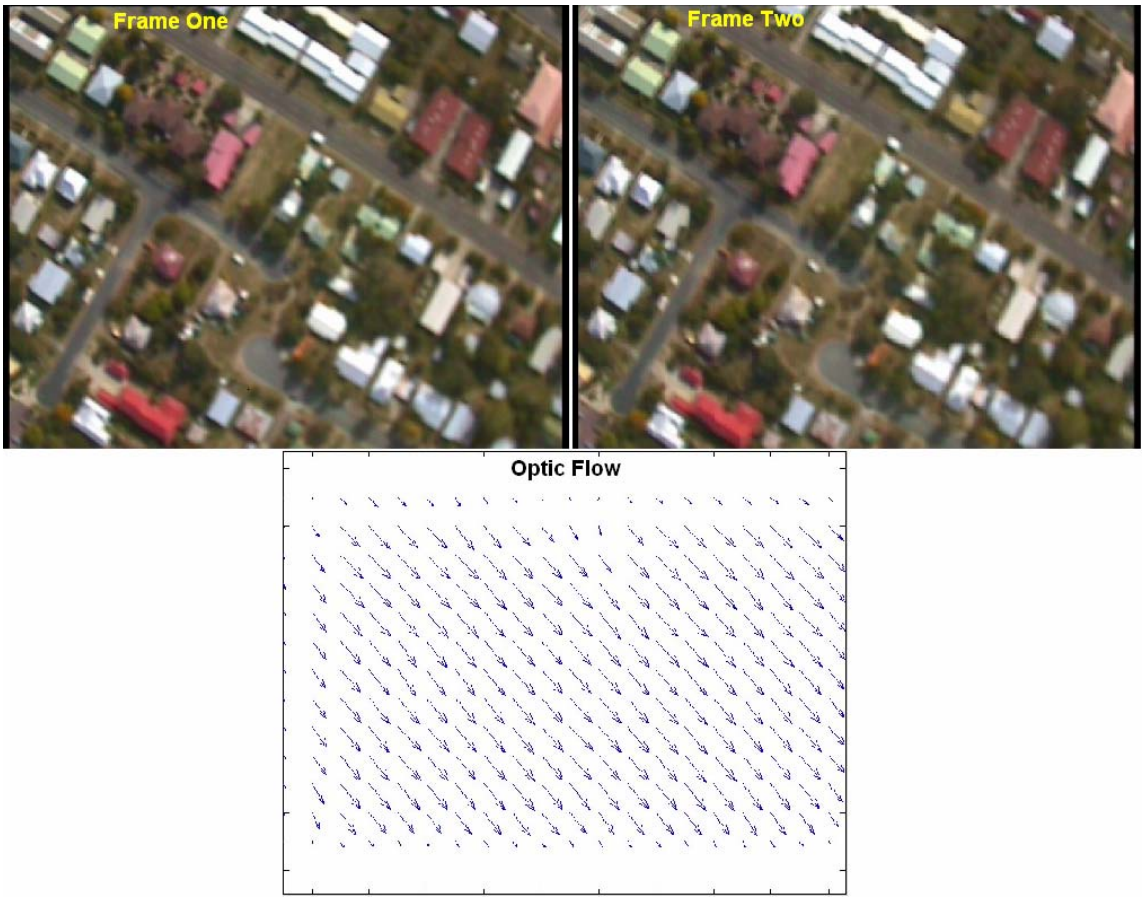

Fig. 2: Optic Flow Example

The output of this processing stage is the complete optic flow map.

It should be noted that this application requires that the camera be aligned to the x body axis of the aircraft. For optic flow calculation there must be some portion of the ground in the field-of-view of the camera. The chance of the ground not being in the field-of-view can be lessened by utilising a camera with a wide-angle lens which would allow the ground to be in view for the expected pitch angles encountered during flight, i.e. maximum expected pitch angle of +/- 30 degrees would require a FOV greater than 60x60 degrees. Due to the sometimes unpredictable nature of flight and physical limitations, the condition of ground in the field of view can not be guaranteed, hence limiting the performance during those periods to GPS derived attitude only.

Pseudo Euler Angle and Rate Calculation

The calculations are based in part on the work done by R. Kornfeld, R. Hansman, and J. Deyst [7, 8] out of which the introduction of pseudo-roll and pseudo-pitch arise.

The three Euler parameter approximations are solved in this stage. They are the pseudo-roll, ϕ_p, pseudo-pitch, θ_p, and pseudo-yaw, ψ_p. These parameters are approximations of the actual roll, pitch and yaw. These are based on the principal that during coordinated flight, distinct relationships exist between the velocity and acceleration as measured by a GPS receiver and these angles. The calculated pseudo-roll closely follows that of the actual roll, where the pseudo-pitch is related to the pitch of the aircraft with an offset of the angle of attack and any wind induced effects. Whilst the pseudo-pitch contains an offset, it directly

relates to the pitch component of the aircraft velocity vector with respect to the local horizon. The components that make up the pitch are illustrated in Fig. 3.

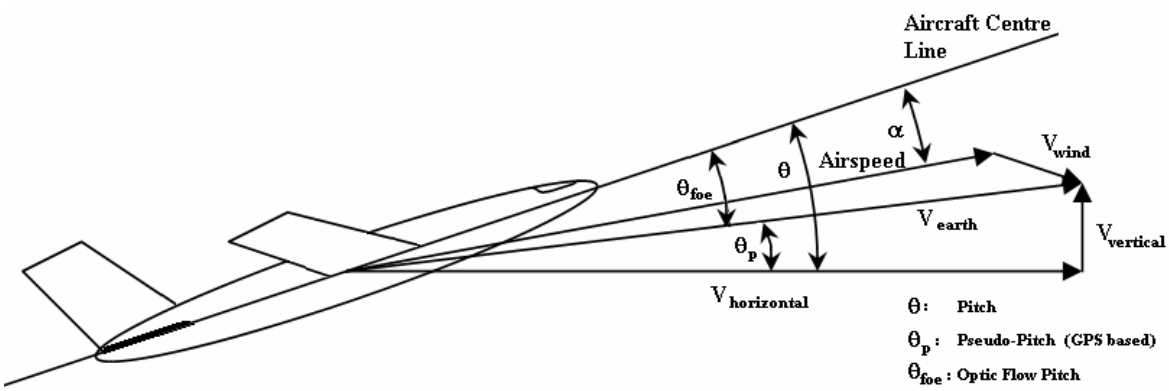

Fig. 3: Pitch Components

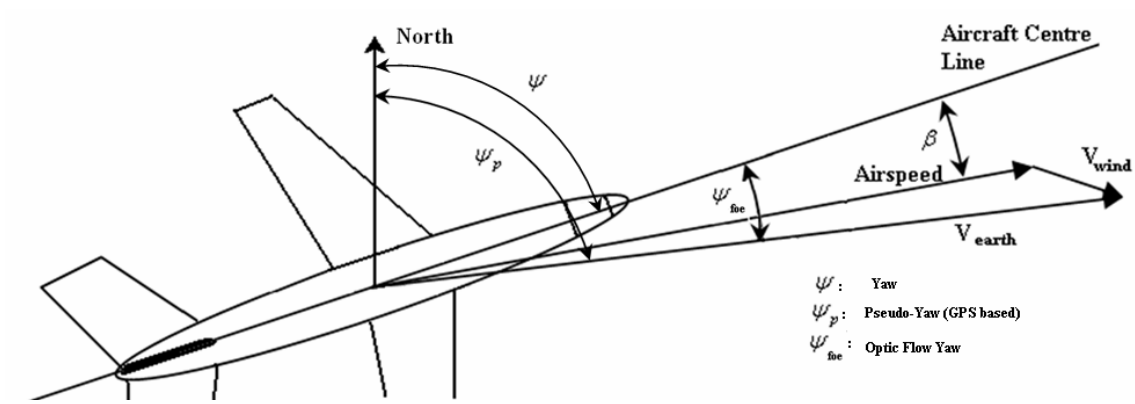

Fig. 4: Yaw Components

The pseudo-yaw is related to the yaw of the aircraft with an offset of the sideslip angle and any wind induced effects. The pseudo-yaw contains an offset but it directly relates the yaw component of the aircraft velocity vector with respect to the horizontal plane of the north east down (NED) coordinate system.

Euler Pseudo-Roll Calculation

The pseudo-roll is calculated based on the combination of the local gravity vector and the pseudo acceleration lift vector, $\widetilde{L}$. The pseudo acceleration lift vector is based on the accelerations derived from the state extrapolation stage using the accurate Doppler based GPS velocity measurements.

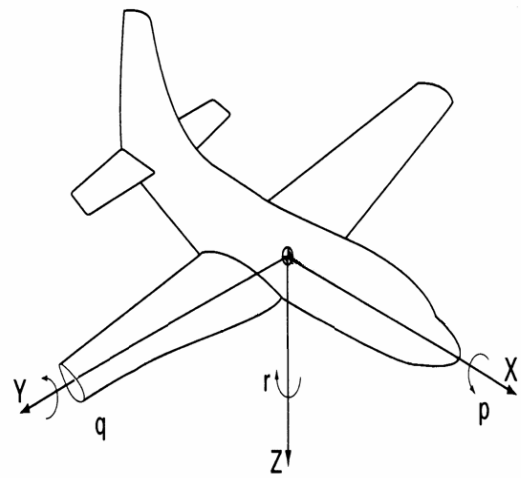

Fig. 5: Aircraft Body Frame

By using the components of acceleration and gravity that lie in the plane normal to the velocity vector, along with the assumption of coordinated flight (velocity vector aligned with the aircraft x axis), we can measure the acceleration force in an approximated y-z plane of the aircraft body frame. The pseudo acceleration lift vector, $\widetilde{L}$, will lie in the approximated y-z aircraft body frame and it represents the direction of the total lift forces acting on the aircraft normal to the body x axis.

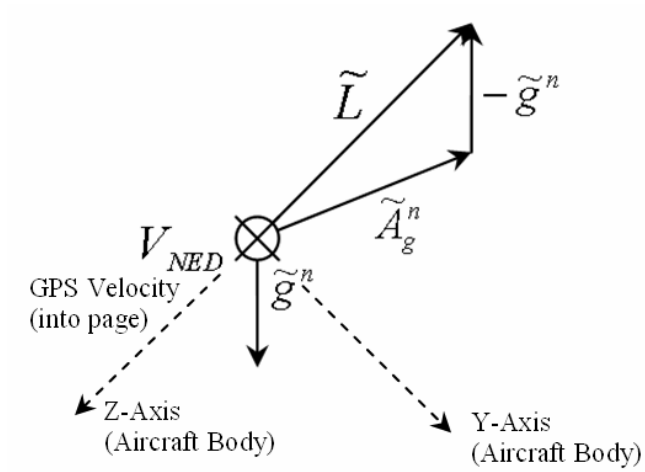

Fig. 6: Determination of Pseudo Acceleration Lift Vector

The direction of the pseudo acceleration lift is dictated by the roll angle of the aircraft and thus provides roll angle information.

The following definitions are used for the calculation of pseudo-roll.
A_{NED} Represents the GPS derived acceleration vector.
$\widetilde{A}_g^n$ Represents the component of the aircraft acceleration vector that lies in the plane normal to the aircraft velocity vector V_{NED} where

$$\widetilde{A}_g^n = A_{NED} - \left(\frac{A_{NED} \cdot V_{NED}}{|V_{NED}|^2} \right) \cdot V_{NED} \; \{m/sec^2\} \tag{1}$$

$\tilde{g}^n$ Represents the component of the gravity acceleration vector that lies in the plane normal to the aircraft velocity vector V_{NED} where

$$\tilde{g}^n = g - \left(\frac{g \cdot V_{NED}}{|V_{NED}|^2} \right) \cdot V_{NED} \; \{m/sec^2\} \tag{2}$$

Using these definitions, we can express the pseudo acceleration lift vector as shown in Eqn 3 and Fig. 6.

$$\tilde{L} = \tilde{A}^n_{NED} - \tilde{g}^n \; \{m/sec^2\} \tag{3}$$

To provide a reference for the pseudo lift vector, the local horizontal reference, $\tilde{p}$, is shown in Fig. 7 and defined with Eqn 4.

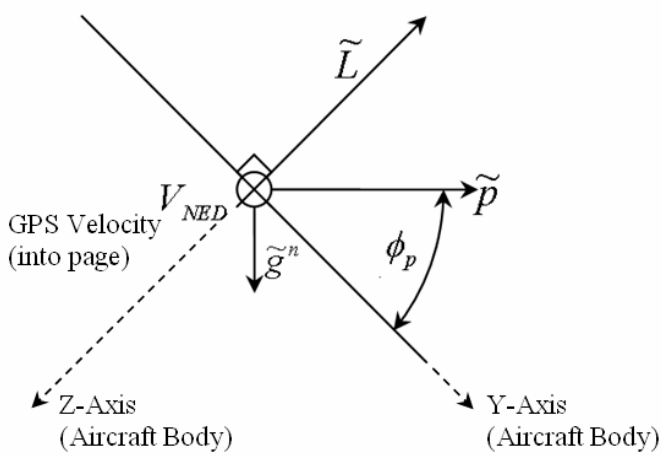

Fig. 7: Determination of Pseudo-Roll

$$\tilde{p} \approx g \times V_{NED} \approx \tilde{g}^n \times V_{NED} \tag{4}$$

The pseudo-roll ϕ_p is calculated as the complement of the angle between the pseudo lift vector, $\tilde{L}$, and the local horizontal reference, $\tilde{p}$, as shown in Eqn 5.

$$\phi_p = \arcsin\left(\frac{\tilde{L} \cdot \tilde{p}}{|\tilde{L}| \cdot |\tilde{p}|} \right) \{rad\} \tag{5}$$

Euler Pseudo-Pitch Calculation

The pseudo-pitch, θ_p, is calculated directly from the velocity vector of the aircraft. As a result, this is an angle representative of the pitch angle of the motion of the aircraft and not of that actual aircraft. We let the subscripts of N, E and D in Eqn 6 and Eqn 7 represent the respective component of the north east down velocity vector.

$$\theta_p = \arctan\left(\frac{-V_D}{\sqrt{V_N^2 + V_E^2}}\right)\{rad\} \tag{6}$$

Euler Pseudo-Yaw Calculation

The pseudo-yaw, ψ_p, is calculated based on the velocity of the aircraft in the horizontal plane. This derivation is simular to the pseudo-pitch in that it is an angular representation based on the motion of the aircraft and not on the actual aircraft.

$$\psi_p = \arctan 2\left(\frac{V_N}{V_E}\right)\{rad\} \tag{7}$$

Euler Pseudo Rate Calculation

For the purpose of disassembling the optic flow it is necessary to have knowledge of the aircraft body rates. To calculate the aircraft body rates, the Euler rates will first be calculated with respect to the local tangent reference frame and then rotated using the pseudo Euler angles to align with the aircraft body frame.

The pseudo Euler roll, $\dot{\phi}_p$, pitch, $\dot{\theta}_p$, and yaw, $\dot{\psi}_p$, rates are calculated by simply taking the derivative wrt time of the Euler angles.

Aircraft Body Pseudo Rate Calculation

With knowledge of the pseudo Euler angles which relate the aircraft body frame to the local tangent frame, the Euler pseudo rates relative to the local tangent frame can be rotated into the aircraft body reference frame with the transform shown in Eqn 8.

$$[pqr] = \begin{bmatrix} \sin\psi_p \cos\theta_p & \sin\psi_p \sin\theta_p \sin\phi_p + \cos\psi_p \cos\phi_p & \sin\psi_p \sin\theta_p \cos\phi_p - \cos\psi_p \sin\phi_p \\ \cos\psi_p \cos\theta_p & \cos\psi_p \sin\theta_p \sin\phi_p - \sin\psi_p \cos\phi_p & \cos\psi_p \sin\theta_p \cos\phi_p + \sin\psi_p \sin\phi_p \\ \sin\theta_p & -\cos\theta_p \sin\phi_p & -\cos\theta_p \cos\phi_p \end{bmatrix} \begin{bmatrix} \dot{\phi}_p \\ \dot{\theta}_p \\ \dot{\psi}_p \end{bmatrix} \tag{8}$$

Optic Flow Disassembly

The optic flow is an accumulation of six individual components, three components each of rotational and translational motion.

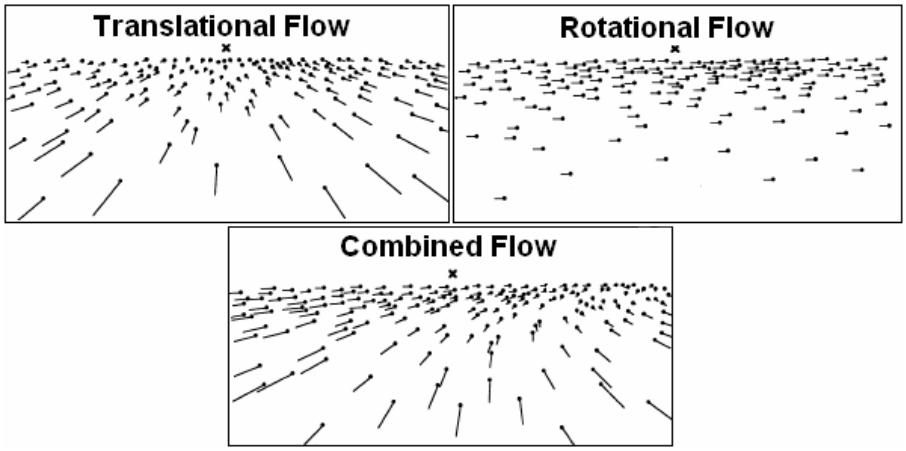

Fig. 8: Optic Flow Component Example[9]

The extraction of these components is necessary for the accurate interpretation of the optic flow data. The dominant component of the optic flow will be the translation along the aircraft x axis, i.e. the direction of motion. With knowledge of the pseudo rates [*pqr*], the rotational components of the optic flow can be removed leaving only the translational motion. Fig. 9 describes the different components of the rotational optic flow and their combined effect.

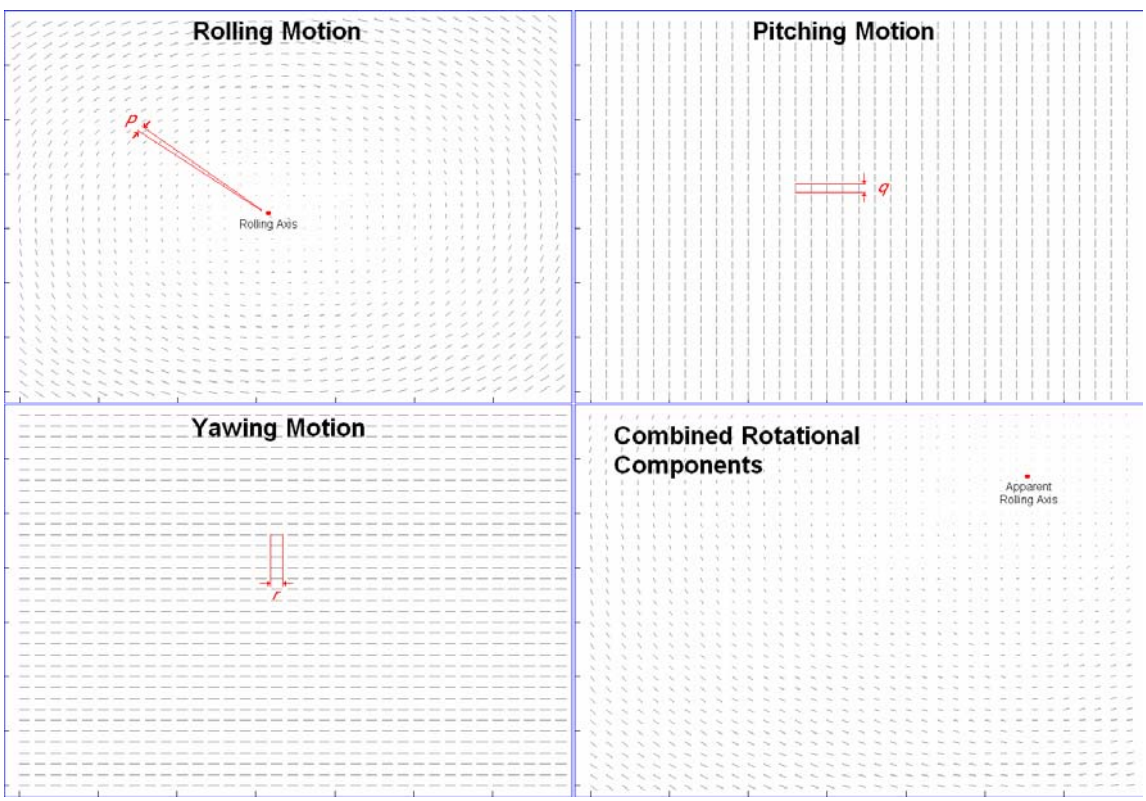

Fig. 9: Rotational Optic Flow

The rotational components of the optic flow are independent of the distance to the object from which the optic flow is being generated. The images shown are a simplified model that does not include the effects of the curvature of the field of view (FOV) and lens distortion. The camera is orientated coincident with the aircraft x axis of the aircraft.

The translational motion direction can be extracted from the image frame by utilising the location of the focus of expansion (FOE) after the removal of the rotational components. The

translational motion magnitude is known from the velocity measurements of the GPS receiver.

FOE in the centre of the FOV indicates that the aircraft is traversing directly along its x axis. Deviations from the centre of the FOV in the vertical direction off the roll angle relate to a z axis translational component. Likewise for the y axis and horizontal displacement coincident to the roll angle from the FOE. The output of this processing stage is a translational optic flow map.

Euler Angle Calculation

The Euler angles are calculated based on the previously derived GPS pseudo attitude and the position of the FOE in the translational optic flow. The translational component of the optic flow provides a method of relating the GPS derived pseudo Euler angles to the aircraft body frame to give a true Euler angle representation. Essentially the translational optic flow gives the offset of the direction that the aircraft is pointing relative to its actual velocity. A simple weighted line intersection voting routine is implemented for identifying the position of the FOE.

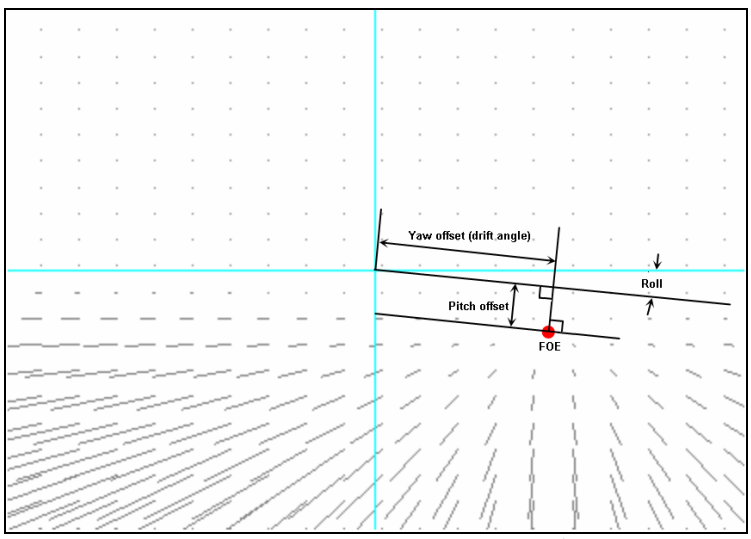

Fig. 10: Velocity Vector Offset[1]

As shown in the results of testing the pseudo-roll very closely matches the actual roll so this value is accepted as the true roll.

The pitch and yaw angle calculation are based on the pseudo attitude combined with the optic flow offset as measured from the translational optic flow map.

Pitch optic flow offset is calculated by measuring the distance of the FOE from the centre of the FOV normal to the roll angle. The GPS derived pseudo-pitch and the optic flow pitch offset is combined to give the true representation of the pitch angle.

The effect of combining the two components of the pitch angle is illustrated in Fig. 11. The combination of the GPS derived pseudo pitch and the optic flow pitch offset produces a close approximation of the true pitch even during undesirable manoeuvres such as a stall.

[1] This figure is only appropriate if the rotational components of the optic flow have been removed.

The optic flow yaw offset is calculated by measuring the distance of the FOE from the centre of the FOV tangential to the roll angle as illustrated in Fig. 10. The optic flow yaw offset is commonly known as the drift angle. The yaw offset is combined with the GPS derived pseudo-yaw to give the true yaw angle of the aircraft.

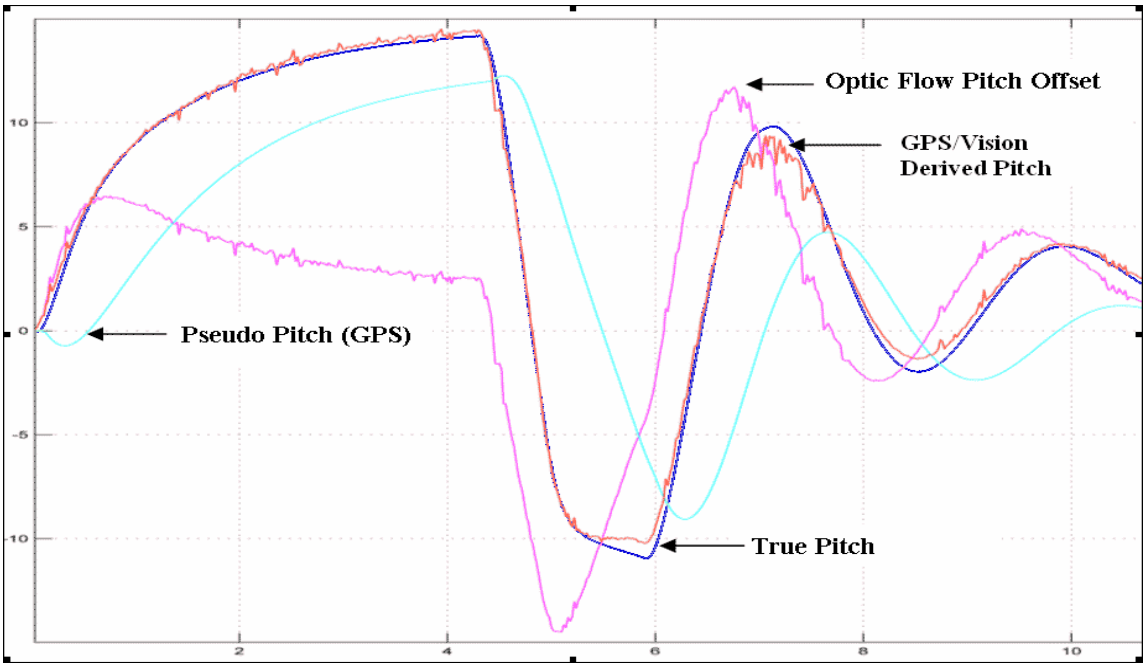

Fig. 11: Pitch Angle

Depth Reckoning

The velocity and line of site direction of the image plane pixels are determined utilising the velocity magnitude from the GPS and the velocity direction from the FOE of the translational optic flow. This information along with the translational optic flow map is then utilised to determine the distance to objects, including the ground if visible, giving a depth map of the objects in the FOV. The following notation will be used for the calculation of the distance to objects.

Ω Represents the magnitude of the optic flow,
D_{LOS} Represents the line of sight vector represented in the north east down frame,
γ Represents the angle between the velocity vector V_{NED} and the line of sight vector D_{LOS} which is calculated with Eqn 9.

$$\gamma = \arccos\left(\hat{V}_{NED} \bullet \hat{D}_{LOS}\right)\{rad\} \tag{9}$$

The optic flow magnitude equation is as follows in Eqn 10.

$$\Omega = \left(\frac{|V_{NED}|}{|D_{LOS}|}\right) \cdot \sin(\gamma) \tag{10}$$

Rearranging Eqn 10 to solve for the unknown magnitude of the line of sight vector yields Eqn 11.

$$\left|D_{LOS}\right| = \frac{\sin(\gamma)\cdot\left|V_{NED}\right|}{\Omega}\ \{m\} \tag{11}$$

An estimation of the height above ground can be made using a knowledge of the camera orientation and the distance to the objects in the field of view. This makes the assumption that the ground is generally level and in the field of view.

By calculating the angle λ between the local horizon and the line of sight vector of a distance measurement D_{LOS}, the altitude above ground level (AGL) estimation can be made using Eqn 12.

$$AGL \approx \left|D_{LOS}\right|\sin(\lambda) \tag{12}$$

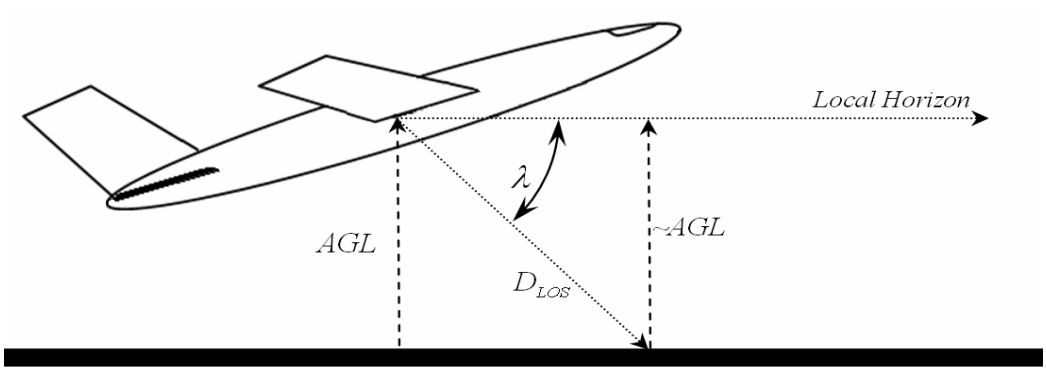

Fig. 12: AGL Estimation

Whilst this AGL estimation is subject to the assumption of level surroundings it would primarily be utilised during the takeoff and landing phases of flight where the surrounding airfield would generally meet this assumption.

The output of this processing stage is a depth map indicating the distance of objects in the field of view and the height above ground if the ground is visible.

Simulation Environment

To facilitate concept validation, algorithm development and testing, a comprehensive simulation environment has been developed. This environment is implemented in Simulink® and is comprised of several logical models as described below,

- Aircraft Model – a six degrees of freedom model that provides the simulated state of an aircraft
- Control Model – provides the control inputs for the aircraft model
- Flight Management Model – provides the control model with the current waypoint information
- Terrain Model – provides a map of distances to the ground in camera pixel coordinates
- Vision Model – provides a optic flow map including errors associated with the optic flow calculation process
- GPS Model – provides the position and velocity that has been degraded to match what would be output from a GPS receiver

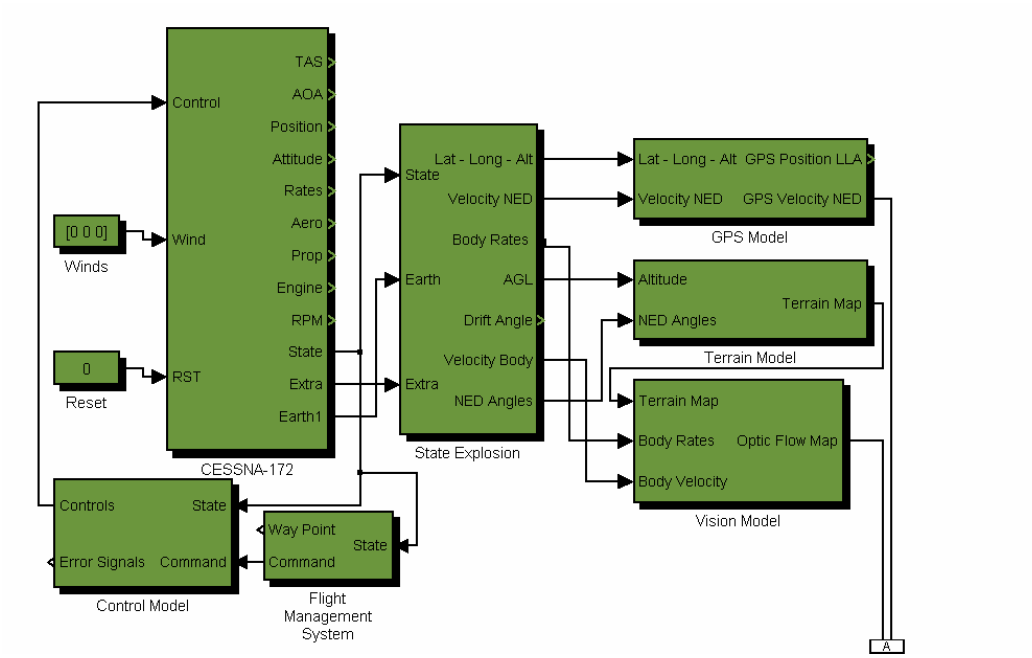

Fig. 13: Aircraft Simulator

The aircraft simulator as illustrated in Fig. 13 is designed to closely model a real aircraft and its sensors. The GPS and Vision model includes errors that are typically found in the output of the respective sensor. The simulated sensor suite implementation is as illustrated in Fig. 14. Inputs to this sensor suite model are GPS velocity and optic flow maps. The optic flow map shown in Fig. 15 is representative of what would be produced by an optic flow algorithm from the image stream.

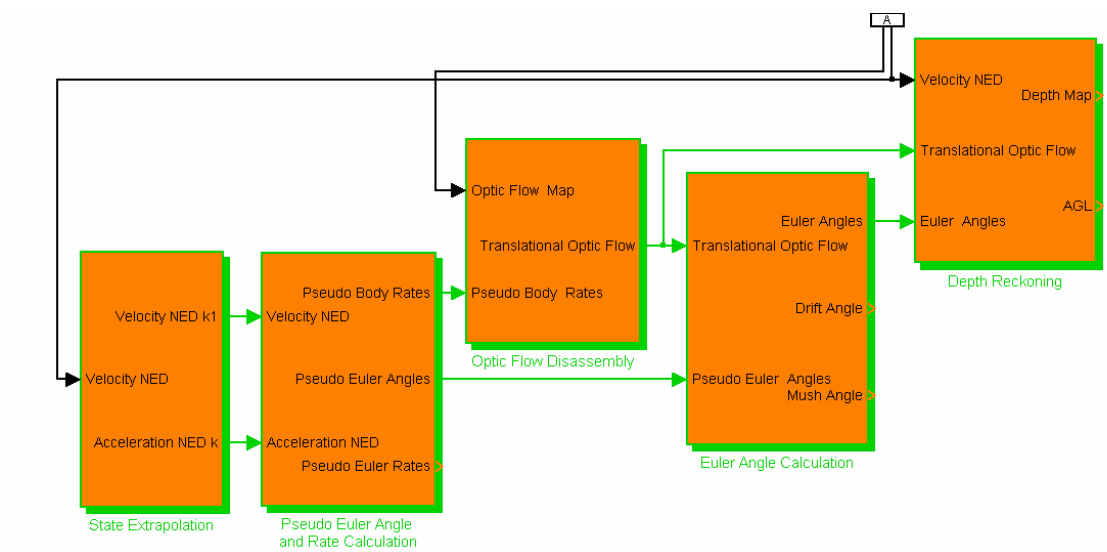

Fig. 14: Sensor suite Simulator

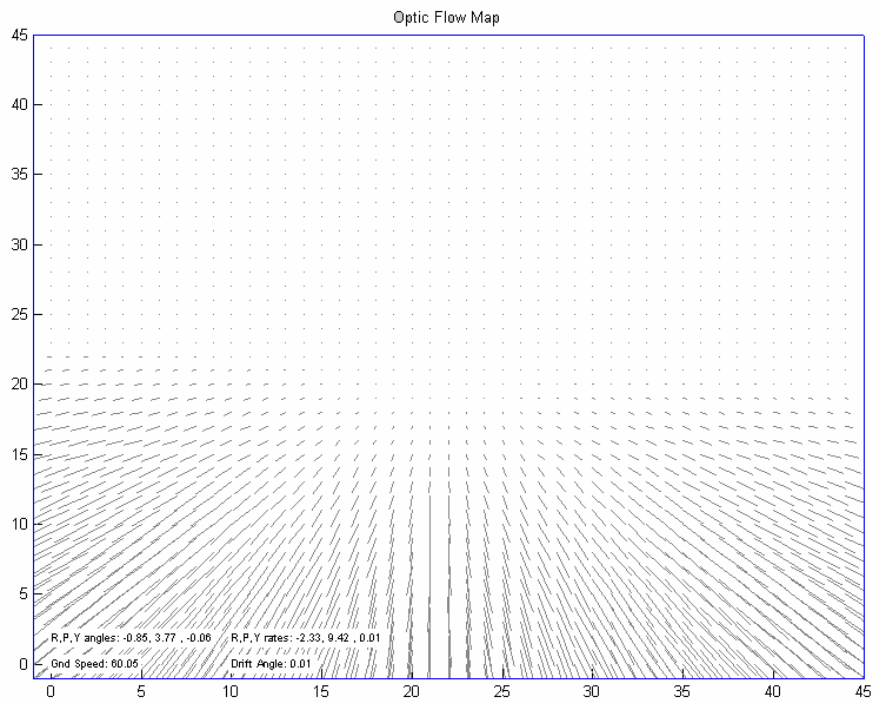

Fig. 15: Optic Flow Map

Results

A reference flight plan has been generated, within the simulation environment, to enable the evaluation of the performance of the proposed sensor suite. The reference flight plan is illustrated in Fig. 16. The results presented in this paper are based upon simulated flights using this reference flight plan. Table 1 summarises the key simulation parameters used in gaining the results presented in this paper.

Table 1: Simulation Flight Parameters

Parameter	Value
Optic Flow Density	45 x 45
Camera Field of View [deg]	90 x 90
Flight Length [sec]	300
Optic flow error [deg]	+/- 2.5

The optic flow error of +/-2.5 degrees has been introduced into that angle of the flow line. This is a value typical found during the optic flow calculation with the algorithm that has been chosen for this research [10].

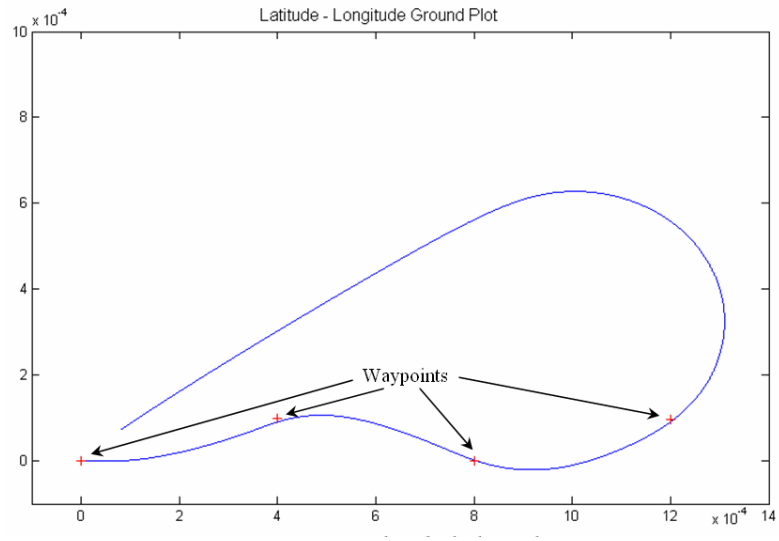

Fig. 16: Simulated Flight Path

A summary of the results gained from the simulated flights are presented in Table 2 which shows that the performance of the sensor suite for Euler angle calculation is of an acceptable level.

Table 2: Euler Angle Error Results

	Roll	Pitch	Yaw
Error Mean [deg]	-0.0276	-0.1400	0.0934
Error Std [deg]	0.1981	0.2872	0.4210

The individual Euler angles are presented below and discussed in turn.

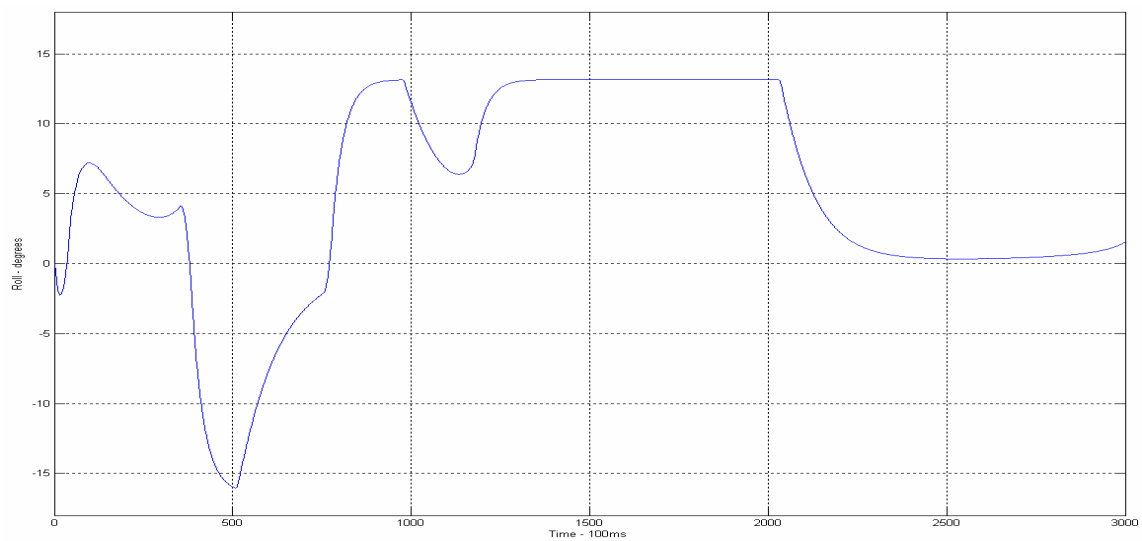

Fig. 17: True Roll Angle

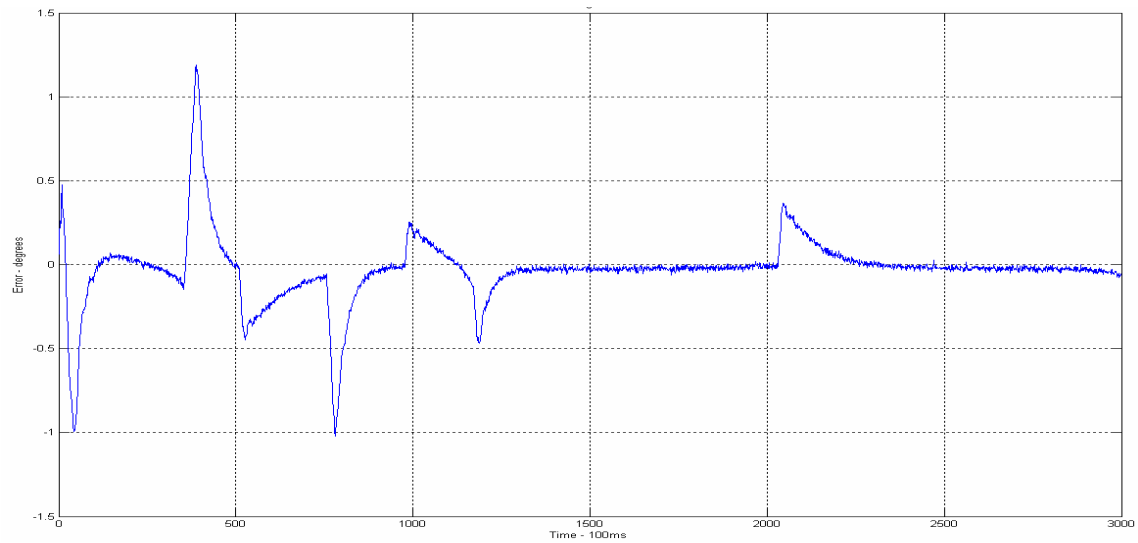

Fig. 18: Roll Angle Error

Fig. 17 shows the true roll experienced during the flight. As can be seen from the roll error shown in Fig. 18, the overall performance gives rise in general to less than ½ degree error, with the exception of some noticeable spikes. The roll is calculated independent of the optic flow measurement and is thus based purely on the GPS velocity. The spikes of error occur in periods of rapid change in roll angle. As the GPS velocity and subsequently derived accelerations are subject to a slight delay inherent with GPS receivers and processing, this error is unavoidable.

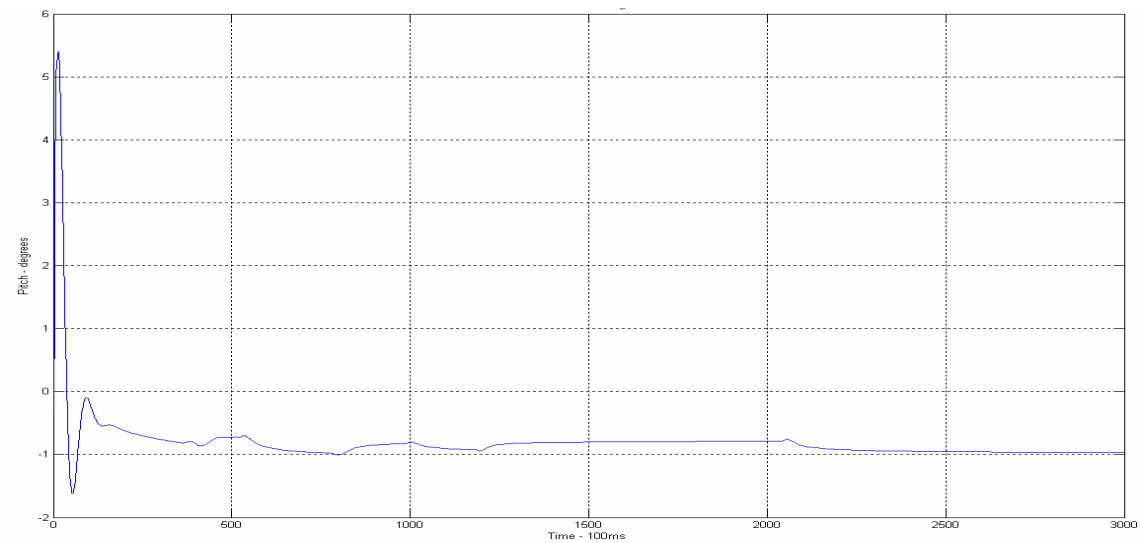

Fig. 19: True Pitch Angle

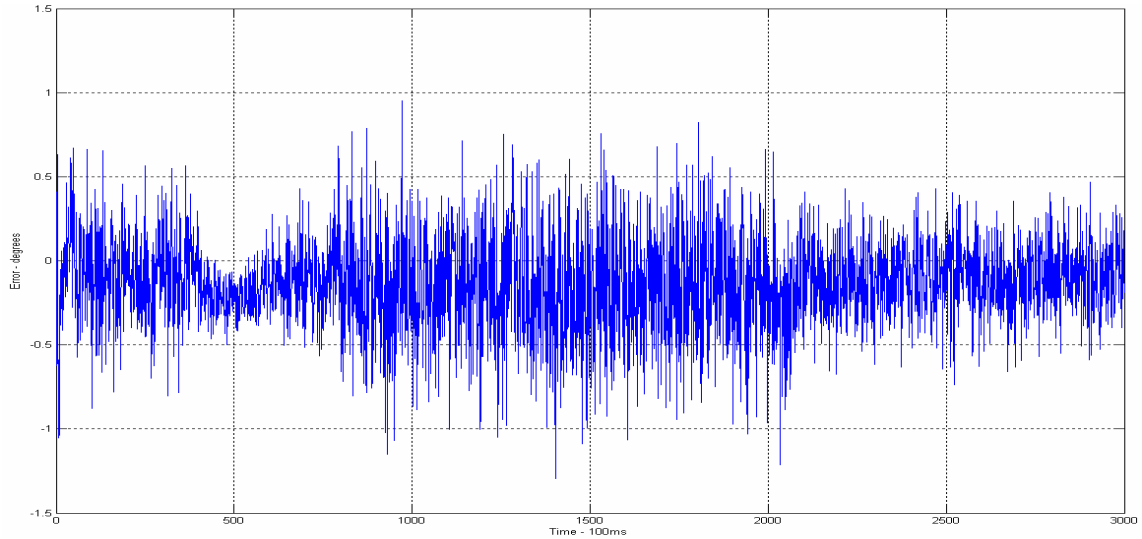

Fig. 20: Pitch Angle Error

Pitch angle for the duration of the flight is shown in Fig. 19. After an initial period of change due to start up of the simulation, equilibrium is reached. The pitch error as shown in Fig. 20 is a distribution bounded by approximately +1/2 to -1 degree of error. The error consists mainly of noise generated by the optic flow pitch offset derivation. There are three main sources of error in calculating the optic flow offset and they are as follows,

- The introduction of noise in the optic flow during generation of the simulated optic flow map. This is done to provide a better representation of what would be calculated from an actual image stream.
- Use of pseudo-rates for removing the rotational components of the optic flow. The only rate measurement available is derived from the GPS and therefore contains error. Due to the predominate portion of the optic flow being translational flow and more specifically translational flow in the x body direction, the rotational components are adequately removed with the pseudo rates for this application. The error that exists due to this is not able to be mitigated.
- The algorithm for the estimation of the focus of expansion is a rudimentary implementation of a weighted line intersection voting routine. This error can be reduced through a filtering regime based upon knowledge of the maximum rates that the UAV would encounter as well as past FOE values.

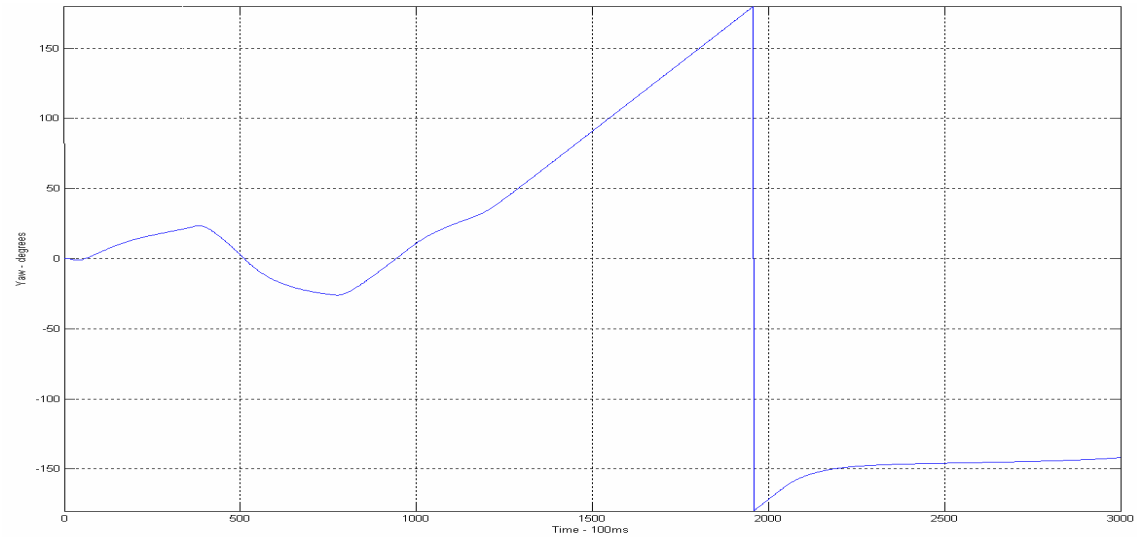

Fig. 21: True Yaw Angle

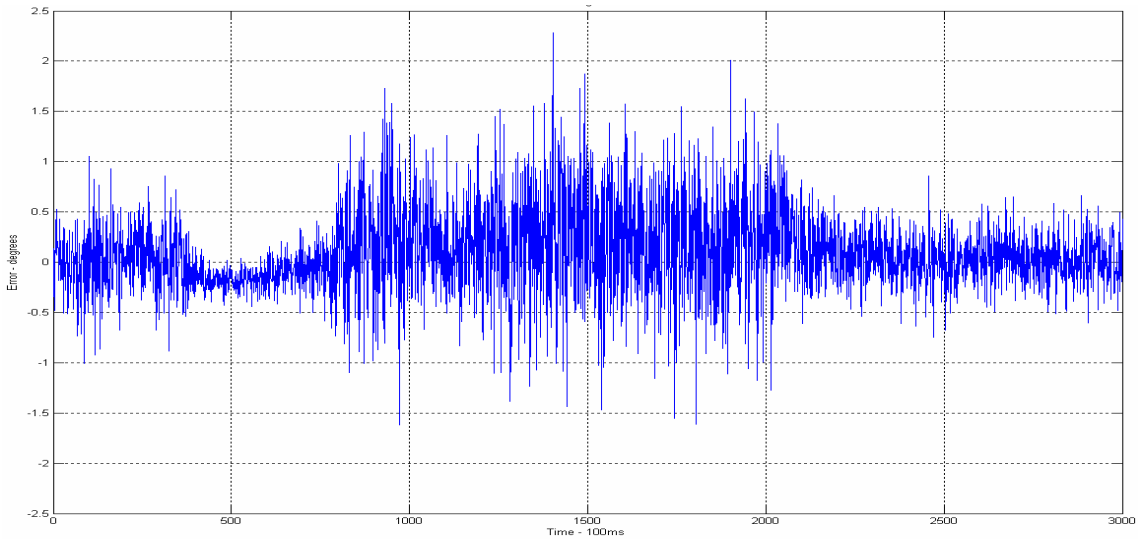

Fig. 22: Yaw Angle Error

Yaw angle error as shown in Fig. 22 has the same characteristics as found in the pitch and this is a result of the same error sources affecting pitch also affecting yaw.

Based upon the results for Euler angle calculation it can be concluded that the concept presented is capable of providing a level of accuracy sufficient for basic UAV operations.

To assess the quality of the height above ground level (AGL) estimation the same flight plan was flown with a commanded reduction in height toward the end of the simulation. The true AGL is shown in Fig. 23.

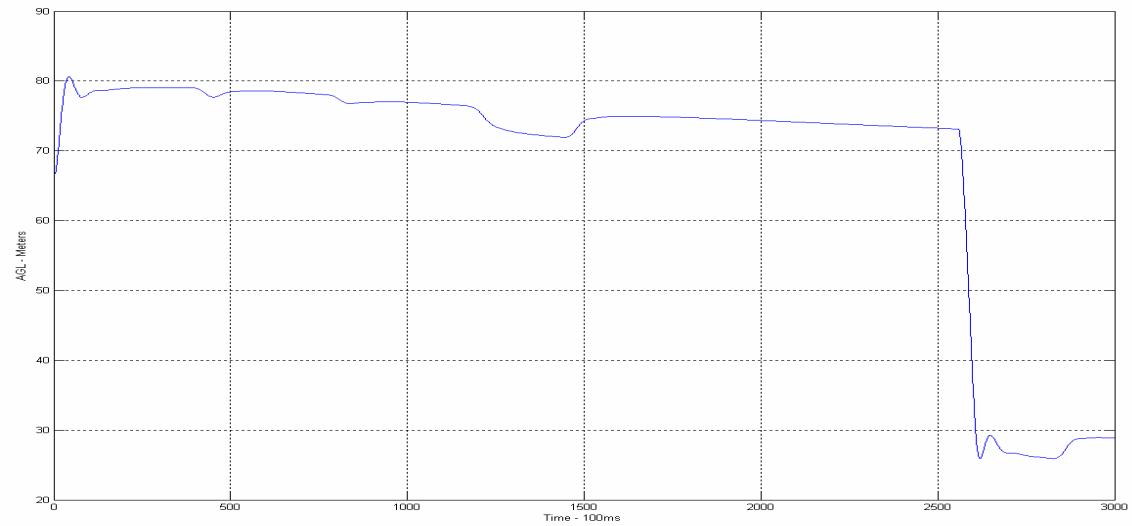

Fig. 23: True AGL

The error for the AGL estimate is illustrated in Fig. 24. The error is such that it can not be reliably used at this stage although the results do show promise. It is noted that the magnitude of the error reduces in the period of the flight where the AGL is smallest. The rudimentary implementation of the AGL estimation algorithm is believed to be the cause of the relatively poor results and future plans are to rectify this. Future implementations will also exploit the knowledge of the UAV attitude in a more rigorous way.

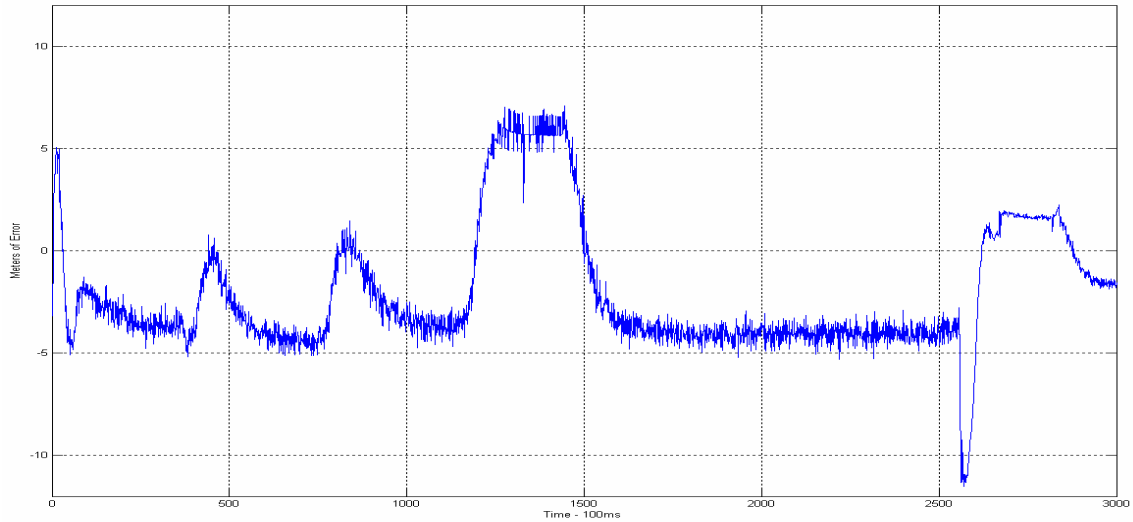

Fig. 24: AGL Error

Discussion

The core objective of this research is to investigate the synergies that exist between GNSS and vision for fixed wing UAV navigation and control applications. This paper presents the research conducted to date in this field.

The proposed research is unique in several aspects,

1. The use of GNSS and biologically inspired techniques (i.e. optic flow) to derive the velocity with respect to the UAV body frame.
2. The use of GPS derived attitude to decouple the rotational and translational components of optic flow
3. The use of a vision based attitude sensor without the need for horizon tracking
4. The use of a vision based navigation sensor providing roll, pitch and yaw

With the fusion of GNSS and vision, an unprecedented level of functionality can be achieved for a given size, mass, cost and power consumption. There are key problem areas that have been overcome to make the proposed sensor suite viable. GNSS can provide an estimate of the attitude, but only of the velocity of the aircraft and not of the aircraft itself. Optic flow can provide a link between the attitude of the aircraft and its velocity. It is this combination that provides the complete attitude information.

Horizon tracking is the traditional approach to attitude determination with a vision sensor but it's shortcoming is that the horizon needs to be in the field of view of the camera. The method described in this paper removes this restriction, providing a more robust attitude measurement than simple horizon tracking.

Optic flow is not usually used in such environments as the translational and rotational motion is difficult to decouple without knowledge of one of them. The use of the GNSS derived attitude provides rotational motion estimates enabling this problem to be overcome.

The translational optic flow is used to determine the direction of travel of the aircraft with respect to the aircraft frame. With this knowledge the translational flow can then be used to determine two parameters, the velocity vector – body frame pitch and yaw offset, and the calculation of the distance to the object from which the optic flow measurement was derived. Distance calculation from optic flow measurements is a function of velocity and the angle of the measurement off the velocity vector. The angle can be determined from the translational optic flow itself leaving the velocity magnitude unknown. This problem is overcome with use of the velocity magnitude from the GNSS sensor.

It is this synergy of the GNSS and vision throughout the sensor suite that facilitates the determination of the wide variety of information.

The results presented for attitude show that estimates can be obtained within the simulation environment of less than one degree error in the mean and standard deviation.

Further development of this sensor suite is continuing with the intent to be able to provide estimates of glide slope, time to impact/touchdown and impact/touchdown position estimation. The inclusion of airspeed in this sensor suite is being investigated with the expectation that this will allow the derivation of the wind vector, angle of attack and angle of sideslip. The limitations on the system, such as requiring the ground to be in the field-of-view for optic flow calculation and noise from GNSS velocity differentiation for the pseudo-roll calculation, will be explored in detail to assess there impact on the overall system.

Conclusion

This paper presents a novel combination of GNSS and vision for UAV navigation and control. The synergies that exist between these two sensors and the information that can be exploited is explored and presented. The motivation for this research was the belief that both GNSS and vision will be integral features of future UAV avionics architectures, GNSS for basic aircraft navigation and vision for obstacle, and aircraft collision avoidance.

The sensor suite concept has been implemented into a simulation environment and results have been presented in this paper. The results show promise in that accuracies of approximately +/- 1 degree are achievable for Euler angles within the simulation environment.

This design has the potential to be superior to other vision based methods used for UAV applications in terms of accuracy, robustness and available information. This research is in the early stages and the methods utilised will be refined and improved as well as validated with data collected from real flights.

Acknowledgements

This work was carried out in the Cooperative Research Centre for Satellite Systems with financial support from the Commonwealth of Australia through the CRC Program.

This research was supported in part by a grant of computer software from QNX Software Systems Ltd.

References

[1] S. Ettinger, M. Nechyba, P. Ifju, and M. Waszak, "Vision-Guided Flight Stability and Control for Micro Air Vehicles," 2004.

[2] R. Causey, "A Lateral Vision-based Control Autopilot for Micro Air Vehicles Using a Horizon Detection Approach," in *Mechanical and Aerospace Engineering*. Florida: University of Florida, 2003, pp. 59.

[3] G. Barrows, J. Chahl, and M. Srinivasan, "Biomimetic Visual Sensing and Flight Control," presented at Bristol Conference on UAV Systems, 2002.

[4] G. Barrows and C. Neely, "Mixed-Mode VLSI Optic Flow Sensors for In-Flight Control of a Micro Air Vehicle," *Critical Technologies for the future of Computing*, vol. 4109, 2000.

[5] G. Barrows, "Future Visual Microsensors for Mini/Micro-UAV Applications," presented at 7th IEEE International Workshop on Cellular Neural Networks and their Applications, 2002.

[6] C. Neustaedter, "An Evaluation of Optical Flow using Lucas and Kanade's Algorithm," 2002.

[7] R. Kornfeld, R. Hansman, and J. Deyst, "Preliminary Flight Tests of Pseudo-Attitude Using Single Antenna GPS Sensing," presented at 17th Digital Avionics Systems Conference, Seattle, WA, 1998.

[8] R. Kornfeld, R. Hansman, and J. Deyst, "The Impact of GPS Velocity Based Flight Control on Flight Instrumentation Architecture," in *International Center for Air Transport, Department of Aeronautics & Astronautics*. Cambridge: Massachusetts Institute of Technology, 1999, pp. 232.

[9] L. Li and W. Warren, "Perception of Heading During Rotation: Sufficiency of Dense Motion Parallax and Reference Objects," *Vision Research*, vol. 40, pp. 3873-3894, 2000.

[10] J. Barron, D. Fleet, and S. Beauchemin, "Performance of Optical Flow Techniques," *International Journal of Computer Vision*, vol. 12:1, pp. 43-77, 1994.